Available online at www.sciencedirect.com

ScienceDirect

Energy Procedia 59 (2014) 285 – 292

Energy Procedia

European Geosciences Union General Assembly 2014, EGU 2014

Geochemical characterization of the Lower Jurassic aquifer in Berlin (Germany) for aquifer thermal energy storage applications

Daniel Müller *, Simona Regenspurg

GFZ German Research Centre for Geosciences, International Centre for Geothermal Research, 14473 Potsdam, Germany

Abstract

Hydrogeochemical processes associated with the potential seasonal storage of 90 °C hot water in a Lower Jurassic aquifer (Lower Sinemurian / Hettangian stages) in the city of Berlin, Germany, are characterized and evaluated to determine possible sources of mineral precipitation resulting in aquifer damage (clogging). Laboratory leaching tests with material from the sandstone aquifer and the pelitic hanging aquiclude obtained from the wellbore "Am Reichstag 2/98" were conducted over a period of 28 days under anoxic conditions. A hydrogeochemical batch reaction simulation of the leaching test was set up with the commercial software PHREEQC and matched to the experimental results. Laboratory experiments show a strong pH decrease and sulfur mobilization as well as precipitation of reddish-brown iron hydroxides. This is most likely the consequence of pyrite oxidation. PHREEQC simulations can reproduce acidification and hematite precipitation if a minor diffusion of oxygen into the system is assumed.

Peer-review under responsibility of the Austrian Academy of Sciences

Keywords: Aquifer Thermal Energy Storage; hydrogeochemistry; geochemical modeling; Lower Jurassic aquifer; Berlin

1. Introduction

Aquifer Thermal Energy Storage (ATES) systems are a specific type of Underground Thermal Energy Storage (UTES) systems, in which shallow or intermediate aquifers are utilized for seasonal storage of large amounts of thermal energy. To that end, aquifer water is produced, heated up and reinjected into the aquifer. One of the most important issues regarding the reliability and the long-term efficiency of these systems is the effect of elevated temperatures and pressures caused by the production-injection cycles on the hydraulic properties of the storage aquifer (e.g. [1,2]). Generally, porosity and permeability in ATES systems can diminish as a result of mobilization and deposition of fine particles, dissolution or precipitation of minerals, clay swelling or gas trapping (e.g. [3,4,5]). In addition to aquifer clogging, geochemical interactions between pore fluid and matrix can affect pH and redox conditions of the groundwater, resulting in undesirable environmental consequences [6].

In this study, the Lower Jurassic aquifer in the city of Berlin (Germany) is investigated with respect to hydrogeochemical processes associated with hot water storage of up to 90 °C. The geochemical characterization is required to simulate the long-term aquifer storage behavior with a coupled hydraulic-thermal-chemical (HTC) aquifer model.

* Corresponding author. Tel.: +49-331-288-1567; fax: +49-331-288-1450.
E-mail address: daniel.mueller@gfz-potsdam.de

Peer-review under responsibility of the Austrian Academy of Sciences
doi:10.1016/j.egypro.2014.10.379

Nomenclature

A_{surf}	surface area (m²)
E	activation energy (J/mol)
K	equilibrium constant
Q	activity product
R	universal gas constant (J/kg/mol)
T	temperature (K)
a_{H+}	activity of H^+
$k_m^{298.15K}$	rate constant at 25 °C and pH 0 for a mechanism m
n_i	reaction order
p_i, q_i	empirical constants
Ω	mineral saturation index (Ω=Q/K)

2. Materials

2.1. Geology

The German capital Berlin is located in the south-eastern part of the Northeast German Basin. Its deep geologic structure is mainly influenced by tectonic movements of the Permian Zechstein salt in the Late Jurassic and Cretaceous periods. The uplifted Mesozoic sediments were subsequently eroded and are missing on top of salt diapirs [7,8,9]. Cenozoic sediments are undisturbed by salt tectonics and are mainly composed of unconsolidated sands. In the Berlin area, Quarternary and Tertiary sediments contain two to four main freshwater aquifers, which are separated from deeper saline aquifers by the Oligocenian Rupelian clay [10].

The target horizon for the aquifer storage is the Lower Jurassic aquifer (Hettangian and Lower Sinemurian stage), which is the shallowest saltwater horizon in central Berlin. Core samples for mineralogical analysis and hydrogeochemical experiments were obtained from the wellbore "Am Reichstag 2/98" from depths of 310 m ("Sample I") and 287 m ("Sample II") below surface. The formation consists of poorly cemented well-sorted greyish fine sandstones with weakly rounded grains [7]. Figure 1 shows the wellbore profile and the sampling depth. Sample I represents the aquifer material, sample II was taken from the hanging aquiclude located in the transition zone between Lower Sinemurian and Upper Sinemurian sediments. Before analysis, the cored sections had been stored for several years in the core repository of the Berlin geological survey.

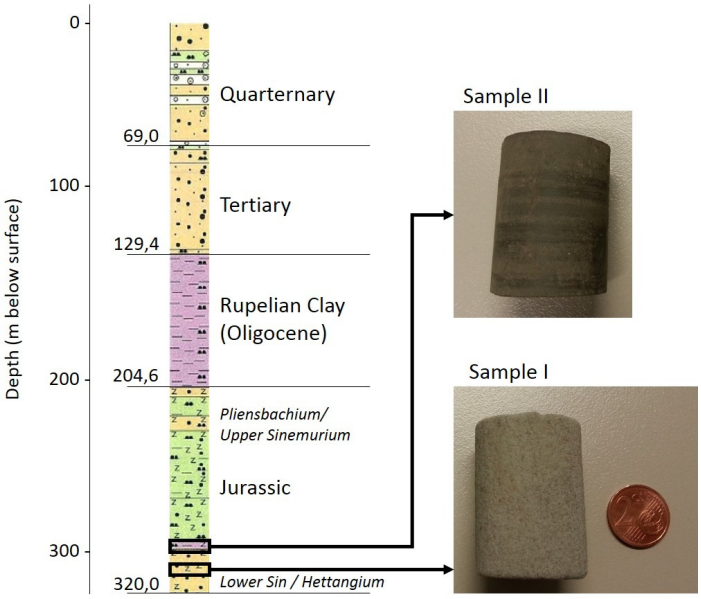

Fig.1. Profile of the wellbore "Am Reichstag 2/98". The sampling depths of sample I (Hettangian / Lower Sinemurian aquifer) and sample II (Sinemurian aquiclude) are marked by black boxes. Profile from [7], modified.

2.2. Groundwater composition

The groundwater chemistry of the Hettangian and Lower Sinemurian aquifer in the Berlin area was described by Huenges using samples from the well "Am Reichstag 2/98" [11]. The average total salinity of the fluid is about 28 g/l, its main ions being sodium (Na) and chloride (Cl) (97 %), and minor ions being magnesium (Mg), calcium (Ca), potassium (K), strontium (Sr), ammonium (NH_4^+), sulfate (SO_4^{2-}), iron (Fe) and manganese (Mn) (figure 2). Small concentrations of carbon dioxide (CO_2) (20 mg/l) and oxygen (O_2) (0 – 0.25 mg/l) are dissolved in the fluid. The dissolved organic carbon (DOC) content is about 3 mg/l. Concentrations of chromium (Cr), nickel (Ni) and copper (Cu) are below 5 µg/l, and of arsenic (As) below 10 µg/l. The average fluid density is 1,018 g/cm³. The pH is neutral, measured values are between 7 and 7.3.

For experiments conducted within this study, a synthetic groundwater was prepared from purified water and 25 g/l >99 % pure NaCl.

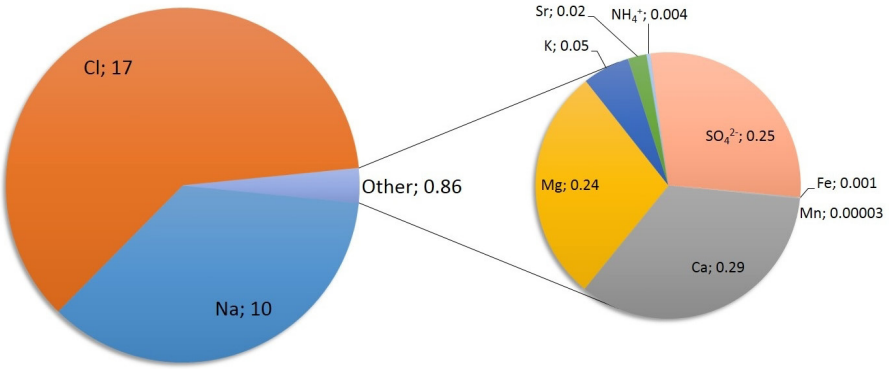

Fig. 2. Main element concentrations (g/l) in the Hettangian and Lower Sinemurian aquifer water. The samples were taken in the well "Am Reichstag 2/98" [11].

3. Methods

3.1. Mineralogical analysis

The mineralogical composition of the rocks was determined by X-ray diffraction (XRD), X-ray fluorescence spectrometry (XRF) and scanning electron microscopy coupled with energy-dispersive X-ray spectroscopy (SEM-EDX). In addition, the specific surface area was measured by Brunauer-Emmett-Teller surface area analysis (BET).

XRD was carried out with a Bruker-axs D8 X-ray Microdiffractometer with GADDS after grinding the grains to a size of 32 µm. Minerals were identified with the software DIFFRAC.EVA, version 2.1. XRF was performed with a PANalytical AXIOS Advanced spectrometer. From the resulting oxide distribution, a set of normed standard minerals was determined using a modified CIPW analysis ([12]), which was adapted to include the mineral phases identified by XRD and EDX. SEM and EDX were realized utilizing a Carl Zeiss SMT Ultra 55 Plus with a tungsten-zircon field emission cathode. The samples were covered with gold for the measurements. Sample I was partitioned by gravitational separation with bromoform (density 2.82 g/cm³) to identify heavy minerals. Minerals were additionally identified by interpreting the EDX spectrograms utilizing reference data from [13]. BET measurements were performed according to DIN-ISO 9277 as a 5-point nitrogen adsorption isotherme by Quantachrome, Odelzhausen (Germany) with a Quantachrome Quadrasorb surface area and pore size analyzer.

3.2. Leaching tests

Laboratory leaching tests were conducted under anoxic conditions with homogenuously ground rock material and synthetic groundwater in PTFE autoclaves ("Bola Hydrolyzing and Digestion Vessels") manufactured by Bohlender. The synthetic groundwater was flushed with nitrogen (N_2) before the experiments to remove dissolved oxygen. A glovebox with argon protective atmosphere was utilized to load the autoclaves under anoxic conditions. Mortared rock from both samples was leached in solid-liquid-ratios (SLR) of 89 g/l and 178 g/l, respectively. The tests were conducted in duplicates. Leaching time was 672 hours (28 days) and the leaching temperature 90 °C. Afterwards, the eluate was filtered (2 µm) and analyzed by inductively coupled plasma optical emission spectroscopy (ICP-OES) for the cations and ion chromatography (IC) for the anions. Electrical conductivity was determined with a WTW TetraCon 325 sensor connected to a WTW Multi 340i data acquisition unit, and pH was measured with a VWR pHenomenal pH 1000L measuring device.

3.3. PHREEQC simulation

The numerical simulation of the leaching tests was conducted with the hydrogeochemical batch reaction code PHREEQC, version 3.1.2. Thermodynamic data was provided by the built-in database file lnll.dat, which had been compiled by the Lawrence Livermore National Laboratory for the geochemical codes EQ3/6 and Geochemist's Workbench [14]. The data therein is based on an extended Debye-Hückel activity formalism and valid in a temperature range between 0 and 300 °C [15]. Additionally, the mass action balance equation for schwertmannite was added to the database from [16].

Reaction kinetics were calculated according to [17]. The rate equation given there integrates neutral, acid and base mechanisms for mineral dissolution. Precipitation can be estimated by reversing the equation or by calculating saturation indices and assuming thermodynamic equilibrium. The rate equation is

$$\frac{dm}{dt} = -A_{surf}\begin{bmatrix} k_{acid}^{298.15K} e^{\frac{-E_{acid}}{R}\left(\frac{1}{T}-\frac{1}{298.15\,K}\right)} a_{H^+}^{n_1}(1-\Omega^{p_1})^{q_1} \\ +k_{neut}^{298.15K} e^{\frac{-E_{neut}}{R}\left(\frac{1}{T}-\frac{1}{298.15\,K}\right)}(1-\Omega^{p_2})^{q_2} \\ +k_{base}^{298.15K} e^{\frac{-E_{base}}{R}\left(\frac{1}{T}-\frac{1}{298.15\,K}\right)} a_{H^+}^{n_3}(1-\Omega^{p_3})^{q_3} \end{bmatrix} \quad (1)$$

Reaction rate constants, activation energies, reaction orders and empirical constants were taken from [17] and the references therein. The reactive surface area is a key parameter for rate calculation in mineral dissolution kinetics since it determines the effective amount of minerals involved in reactions. However, a precise value is often difficult to determine for several reasons [18]. First, specific surface areas of different mineral phases vary by several orders of magnitude. Unless ground and mineral-separated samples are measured, laboratory methods such as BET determine the surface area of the whole rock, which is a combined value of all mineral phases found in the rock. Second, depending on grain packing, mineral paragenesis, coating, and other factors, only part of the mineral surface is exposed to the pore fluid and thus available for reactions. In addition, reactions between pore fluid and mineral surfaces usually occur at selective sites, where etch pits may form [19,20,21]. Consequently, BET surface analysis overestimates the reactive surface area [20]. Third, the morphologies of the mineral surfaces change during reactions, which alters the specific surface area [18]. It is unclear if this affects the actual rate of dissolution, however [21].

In this study, the specific surface area of the rock samples was measured by BET. These values serve as upper boundaries. To determine initial values for the individual mineral phases, literature values from [18,19,22] were used. These initial values were subsequently tuned to the experimental results to get a best match for the actual reactive surface areas. The resulting values for the modeled minerals are given in table 1, in combination with all other required kinetic parameters.

For the simulation, the mineral composition was taken from the XRD, XRF and SEM-EDX measurements, and the fluid composition corresponds to the synthetic groundwater used in the experiments. Initial pH was set to 7, initial pe to -3. Reaction temperature was 90 °C. The reaction was modeled over 672 hours in 28 steps of 24 hours each. All dissolution reactions were modeled using equation (1), while precipitation reactions were modeled assuming thermodynamic equilibrium. Two simulations were conducted to account for possible air leaks in the autoclaves. In simulation 1, 400 µmol of oxygen were assumed to diffuse into the autoclave over 28 days. In simulation 2, no oxygen was allowed to be present in the system.

Table 1. Mineral kinetic rate parameters required for equation (1). Kinetic data is from [17].

Mineral	A_{surf}	Acid mechanism			Neutral mechanism		Base mechanism		
	(m^2/g)	log k	E (kJ/mol)	n_1	log k	E (kJ/mol)	log k	E (kJ/mol)	n_3
Quartz	0.02				-13.4	90.9	-16.29	108.366	-0.5
K-Feldspar	0.01	-10.06	51.7	0.5	-12.41	38.0	-21.2	94.1	-0.823
Albite	0.01	-10.16	65.0	0.457	-12.56	69.8	-15.6	71.0	-0.572
Anorthite	0.01	-3.5	16.6	1.411	-9.12	17.8			
Muscovite	0.10	-11.85	22.0	0.37	-13.55	22.0	-14.55	22.0	-0.22
Kaolinite	2.32	-11.31	65.9	0.777	-13.18	22.2	-17.05	17.9	-0.472
Illite	0.20	-11.31	23.6	0.78	-13.18	35.0	-17.05	58.9	-0.47
Montmorill.	0.20	-12.71	48.0	0.22	-14.41	48.0	-14.41	48.0	-0.13
Ilmenite	0.02	-8.35	37.9	0.421	-11.16	37.9			
Pyrite	0.02	-7.52	56.9	0.5	-4.55	56.9			

4. Results

4.1. Mineralogy

The average mineral composition calculated from XRD and XRF data is shown in figure 3 for both samples. Sample I is a sublithic arenite according to the classification of sandstones by Dott & Folk, and mainly consists of quartz, feldspars, mica and

kaolinite. Trace minerals constitute less than one percent of the total mass. Rutile and Ilmenite were identified by SEM-EDX. The XRF detected 0.035% carbon (C) and 0.06 % sulfur (S) in the samples, which could not be attributed to any mineral phase identified by SEM-EDX or XRD. The carbon originates either from unidentified carbonates or from organic matter. In addition to these trace minerals, gravitational separation of the sample yielded 0.03 % heavy minerals with a density above 2.82 g/cm³, which consist of zircon, tourmaline, staurolite, aluminosilicates and elemental copper.

Sample II is a pelitic rock mainly composed of quartz, k-feldspars, plagioclase, mica and clay minerals. A precise mass distribution of kaolinite, illite and montmorillonite could not be realized with the available data, therefore all clay minerals were merged into a single category. Ilmenite and rutile were identified with SEM-EDX. The XRF spectroscopy detected 1.47 % carbon and 0.76 % sulfur. All sulfur was assumed to be bound in pyrite, as verified by SEM-EDX. Carbon content was associated to calcite, which had been detected by SEM-EDX, and presumably other unidentified carbonates as well as organic matter.

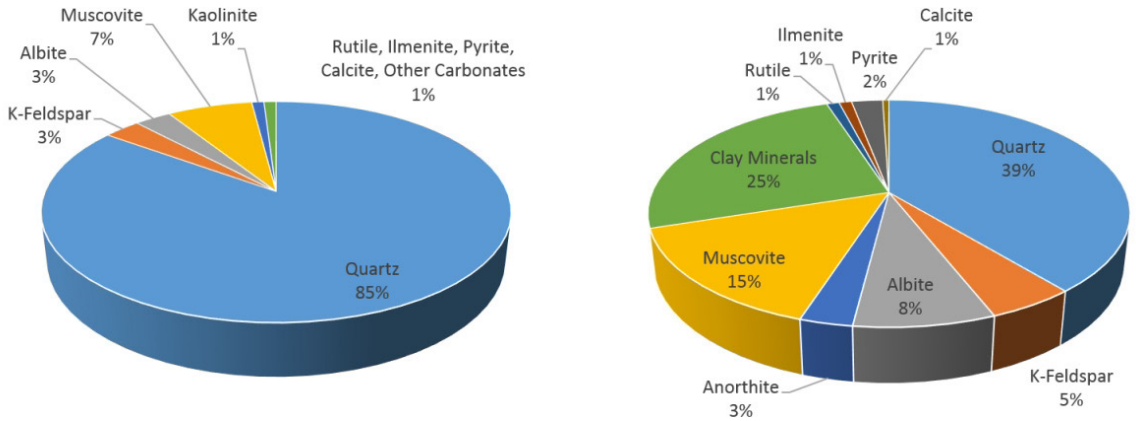

Fig. 3: Mineral distribution estimated from XRD, XRF and SEM-EDX, (a) sample I (b) sample II.

4.2. Ion mobilization

A thin layer of reddish to brown precipitates formed on the inner walls of all autoclaves or was suspended in the liquid. The precipitates were of orange-red (sample I) and muddy-brown (sample II) color (figure 4). In all cases, fluid conductivity increased, and the pH values decreased. For sample I, pH values dropped from an initial value of 7 to 3 (SLR 178 g/l) and 3.3 (SLR 89 g/l), and electrical conductivity increased from 40.4 mS/cm to 42.0 (SLR 178 g/l) and 40.7 mS/cm (SLR 89 g/l), respectively. Main cations in the liquid were Ca, Si, Mg, Fe, Al and K, and the dominant anion was sulfate with only traces of carbonate, phosphate and bromide (table 2). The specific surface area measured by BET decreased from 0.5 m²/g to 0.42 m²/g.

In the sample II extracts, the pH values dropped from an initial value of 7 to 4.1 (SLR 178 g/l) and 4.7 (SLR 89 g/l), and electrical conductivity increased from 40.4 mS/cm to 43.2 (SLR 178 g/l) and 41.8 mS/cm (SLR 89 g/l), respectively. Again, Fe, Si, K, Ca and Mg were the dominant cations in the fluid, but the Al concentration was below the detection limit of the ICP-OES. Sulfur was the main anion, with traces of carbonate, phosphate and bromide (table 2). The specific surface area increased from 13.2 m²/g to 16.5 m²/g.

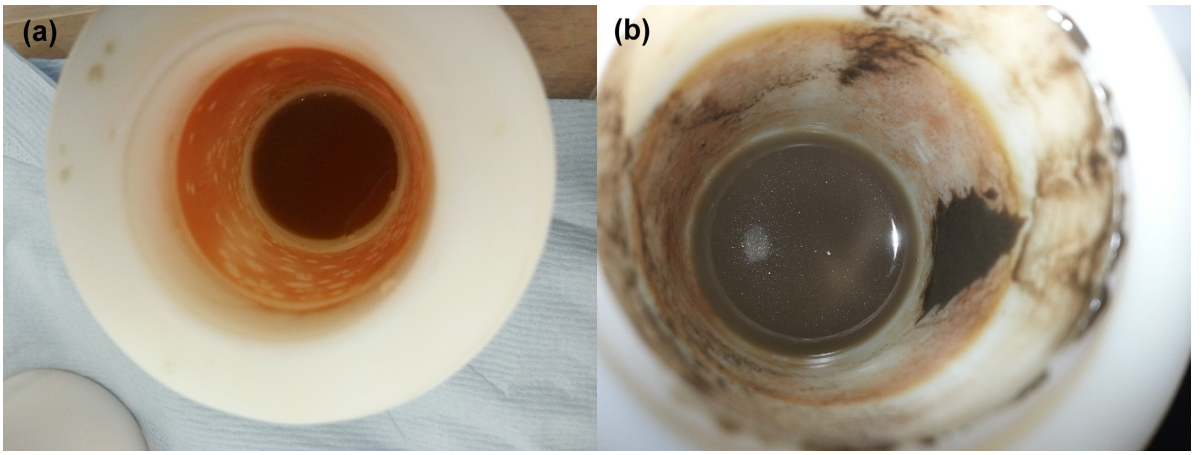

Fig. 4: Precipitates on the inner autoclave walls and in the liquids, (a) sample I (b) sample II.

4.3. PHREEQC simulation

The best fit for the simulations was obtained by assuming pyrite oxidation to occur. This explains the decreased pH value, the release of sulfuric acid, the increased amounts of iron and sulfate in solution and the precipitation of iron bearing minerals as indicated by the reddish color.

Precipitates from sample I were calculated to be hematite, when oxygen was included in the autoclave reaction. In this case, the pyrite oxidation rate was accelerated and more iron and sulfur were dissolved. Sodium and magnesium were not mobilized at all, and potassium was underestimated by one order of magnitude. Silicium and aluminium concentrations matched the order of magnitude of the experiments. The pH decreased to 2.3 (SLR 178 g/l) and 2.6 (SLR 89 g/l), respectively. If no oxygen was present during the reaction, hematite did not become oversaturated and the pH value decreased to slightly acidic values of 6.1 (SLR 178 g/l) and 6.2 (SLR 89 g/l), respectively (table 2).

In sample II, calculations did not show iron mineral precipitation, regardless of the presence or absence of oxygen. The concentration of dissolved iron was two orders of magnitude higher than measured in the experiments. The concentrations of sodium and potassium were underestimated by one order of magnitude, the concentration of magnesium by two orders of magnitude. Silicium matched the experimental results. The pH decreased to 3.5 (SLR 178 g/l) and 3.2 (SLR 89 g/l), respectively. Without oxygen addition, the pH increased to slightly alkaline values of 8.4 (SLR 178 g/l) and 8.1 (SLR 89 g/l) (table 2).

Table 2. Main cations, anions, pH and electric conductivity measured in the eluates after the leaching tests and calculated in PHREEQC simulations. Samples are differentiated by the solid-liquid-ratios (SLR) in which the experiments were conducted. "EXP" marks experimental results, "SIM +O_2" marks simulation results with 400 µmol oxygen added, "SIM" marks simulation results under anoxic conditions. For the experiments, concentrations are given as arithmetic means with standard deviation; missing values for standard deviation are due to only one sample being available for measurements.

Sample,		Concentrations (mg/l)							Conductivity	pH
SLR (g/l)		Ca	Fe	Mg	Si	K	Al	S(6)	(mS/cm)	
I, 178	EXP	15.5±0.7	3.15±0.35	9.00±0.28	15.0±0.0	6.90±1.70	3.10±0.28	42.6	42.0±0.1	3.0±0.0
	SIM +O_2	0	2.8e-3	0	11.0	0.94	4.73	148	n.a.	2.3
	SIM	0	0.11	0	12.9	0.06	0.21	2.4e-4	n.a.	6.2
I, 89	EXP	7.25±0.21	0.76±0.20	4.50±0.14	8.40±0.71	3.50±0.00	1.30±0.28	22.3	40.7±0.4	3.3±0.1
	SIM +O_2	0	5.1e-4	0	6.09	0.59	2.54	74.1	n.a.	2.6
	SIM	0	0.06	0	8.95	0.04	0.20	1.7e-4	n.a.	6.1
II, 178	EXP	738±14	1.90±0.28	76.5±2.1	18.5±0.7	38.5±0.7	<1	536	43.2	4.7
	SIM +O_2	82.8	156.8	0.13	7.74	1.123	0.46	170	n.a.	3.5
	SIM	15.6	4.3e-4	1.5e-5	28.4	1.68	0.63	1.6e-4	n.a.	8.4
II, 89	EXP	407	5.30	44.0	18.0	23.0	1.4	328	41.8	4.4
	SIM +O_2	70.0	153	0.07	6.62	0.65	2.94	169	n.a.	3.2
	SIM	7.84	1.3e-3	2.4e-4	19.1	0.76	0.41	1.6e-4	n.a.	8.1

5. Discussion

The major part of both rock samples consists of weakly reactive minerals, such as quartz, feldspars and mica. The mass fraction of minerals or amorphous phases that are highly reactive is as low as 1 % for sample I and 2 % for sample II. Comparison of data from XRF spectroscopy and fluid analysis of the eluate show a strong mobilization of sulfur. From both samples, approximately 40 % of the sulfur contained in the rock material was mobilized. Additional sulfur may be contained in the precipitates. In a first approximation, the sulfur-bearing mineral of the rock is assumed to be pyrite, which was identified by SEM-EDX in sample II. Since pyrite oxidation is a highly acidifying process, its presence could explain the measured decrease of the pH during the experiments. However, it cannot be excluded that there are other sulfur-bearing minerals, such as Greigite (Fe_3S_4) or amorphous phases, present in the samples.

The precipitates found on the inner walls of the autoclaves are most likely ferrous oxides or hydroxides. Fe^{3+} ions in aqueous solutions can precipitate as goethite (FeOOH) or hematite (Fe_2O_3), releasing protons [23]

$$Fe^{3+} + 2H_2O \Leftrightarrow FeOOH + 3H^+ \quad (2)$$

$$2Fe^{3+} + 3H_2O \Leftrightarrow Fe_2O_3 + 6H^+ \quad (3).$$

The formation of goethite and hematite is considered to be preceded by the formation of amorphous ferrihydrites. The rates of transformation and the ratio of resulting goethite and hematite depend on reaction kinetics. Precipitation of hematite is favored by high temperatures, high ionic strength of the water, and neutral or very low pH [23]. Consequently, the elevated experimental temperatures favor a rapid formation of crystalline goethite and hematite. In terms of pH, sample I favors the formation of hematite over goethite, while sample II provides favorable conditions for goethite precipitation. Furthermore, the presence of secondary ions facilitates the formation of metastable minerals which transform to hematite or goethite over time. In the presence of sulfate, the iron(III)-oxyhydroxysulfate Schwertmannite ($Fe_8O_8(OH)_6SO_4$) precipitates [16]

$$8Fe^{3+} + ySO_4^{2-} + (12 - y + 0.5x)H_2O \Leftrightarrow Fe_8O_8(OH)_x(SO_4)_y + (24 - 2y)H^+ \quad (4).$$

The numerical simulations show that pyrite dissolution is strongly dependent on the availability of oxygen. Assuming a perfectly closed system, no ferrous oxides or hydroxides precipitate. However, even the diffusion of small amounts of O_2 into the system accelerates pyrite oxidation notably. In sample I, this results in the precipitation of iron minerals and an acidification of the solution. In sample II, no precipitation of iron minerals is calculated, regardless of the oxygen content. However, the concentration of sulfur is slightly underestimated while the concentration of iron is overestimated by two orders of magnitude. This suggests that iron was removed from the solution during the experiments, which is supported by the coating found inside the autoclaves. Since the llnl database includes only the reaction of pyrite with water [14]

$$FeS_2 + H_2O \Leftrightarrow 0.25H^+ + 0.25SO_4^{2-} + Fe^{3+} + 1.75HS^- \quad (5),$$

other scenarios that do not involve the diffusion of air into the system are possible. Pyrite may be oxidized by Fe^{3+}, or the reaction may be microbially catalyzed by iron- and sulfur-oxidizing bacteria such as *Thiobacillus ferrooxidans* (e.g. [24]). Schwertmannite is undersaturated in both samples, because the sulfur concentration is too low. Acceleration of pyrite oxidation could result in oversaturation and precipitation of this mineral.

6. Conclusions and outlook

Although the investigated rock samples consist of mainly inert minerals, less than 1 % of highly reactive sulfur-bearing minerals, presumably pyrite, generate precipitations of ferrous oxides and hydroxides that may lead to aquifer clogging. In addition, those reactions release protons, which will decrease the pH of the aquifer water. Oxygen is a key parameter in this process, and preventing O_2 diffusion into the system is required to avoid aquifer damage by chemically clogging the pores of the rock.

An approximate reproduction of the laboratory leaching tests with PHREEQC is possible, but requires further refinement. Particularly, oxidization of pyrite and precipitation of ferrous oxides and hydroxides are complex processes which are difficult to model and quickly become computationally expensive. For coupled reactive flow simulations however, complexity needs to be kept to a minimum to maintain reasonable computation times.

Acknowledgements

This work was performed in the framework of the project „Efficiency and reliability of energy systems in urban districts with seasonal energy storage in aquifers (Aquifer Thermal Energy Storage ATES Berlin)" and is funded by the Federal Ministry for Economic Affairs and Energy (BMWi, 03ESP409A).

The authors would like to thank all members of the ATES project group at the GFZ German Research Centre for Geosciences and the TU Berlin for their valuable contributions to this work. For their mineralogical expertise and help, thanks go to Fiorenza Deon, Hans-Jürgen Förster and Andrea Förster. For valuable assistance on PHREEQC, we wish to thank Dejene Legesse Driba. Furthermore, warm thanks are due to Alexander Limberg (Berlin geological survey) for providing the core material, Rudolf Naumann for performing XRD and XRF analyses, Helga Kemnitz and Ilona Schäpan for carrying out the SEM-EDX analysis, Juliane Herwig for her support on microscopy, Sabine Tonn for conducting ICP-OES analyses, Andrea Vieth-Hillebrand and Kristin Günther for conducting the ion chromatography, and Mashal Alawi and Oliver Burckhardt for providing a glovebox and friendly user support.

References

[1] Seibt P, Kabus F, Wolfgramm M, Bartels J, Seibt A. Monitoring of Hydrogeothermal plants in Germany – an Overview. Proceedings of the World Geothermal Congress 2010, Bali, Indonesia, 25 – 29 April 2010.
[2] Lee KS. A Review on Concepts, Applications, and Models of Aquifer Thermal Energy Storage Systems. Energies 2010; 3: 1320-1334.
[3] Seibt P, Wolfgramm M. Practical Experience in the Reinjection of Thermal Waters Into Sandstone. Proceedings of the Workshop for Decision Makers on Direct Heating Use of Geothermal Resources in Asia Organized by UNU-GTP, TBLRREM and TBGMED in Tianjin, China, 11-18 May 2008.
[4] Ungemach P. Reinjection of cooled geothermal brines into sandstone reservoirs. Geotherm 2003; 32: 743-761.
[5] Ochi J, Vernoux JF. Permeability decrease in sandstone reservoirs by fluid injection: Hydrodynamic and chemical effects. J Hydrol 1998; 208: 237-248.
[6] Palmer CD, Cherry JA. Geochemical reactions associated with low-temperature thermal energy storage in aquifers. Can Geochem J 1984; 21: 475-488.
[7] Rockel W, Brandt W, Seibt P. Ein mesozoischer Aquifer im Zentrum Berlins als saisonaler Wärmespeicher für Parlamentsbauten. Brandenburgische geowiss Beitr 1999; 6: 91-101.
[8] Sippel J, Fuchs S, Cacace M, Braatz A, Kastner O, Huenges E, Scheck-Wenderoth M. Deep 3D thermal modelling for the city of Berlin (Germany). Environ Earth Sci 2013; 70: 3545-3566.
[9] Kahnt R, Ertel S, Feldmann H, Behnke A. Potenzialstudie zur Nutzung der geothermischen Ressourcen des Landes Berlin (Modul 2). Abschlussbericht zu den Ergebnissen. Halsbrücke: GEOS Ingenieurgesellschaft; 2011.
[10] Limberg A, Thierbach J. Hydrostratigrafie von Berlin – Korrelation mit dem Norddeutschen Gliederungsschema. Brandenburgische Geowiss Beitr 2002; 9: 65-68.
[11] Huenges, E. Thermische Untergrundspeicher in Energiesystemen: Optimierung der Einbindung der Aquiferspeicher in die Wärme- und Kälteversorgung der Parlamentsbauten im Berliner Spreebogen:Abschlussbericht; Berichtszeitraum 01.09.2005 – 31.10.2011. Potsdam: Helmholtz-Zentrum Potsdam GFZ Deutsches Geoforschungszentrum; 2011.
[12] Cross W, Iddings JP, Pirsson, LV, Washington, HS. A Quantitative Chemico-Mineralogical Classification and Nomenclature of Igneous Rocks. J Geol 1902; X (6): 555-690.
[13] Reed SJB. Electron Microprobe Analysis and Scanning Electron Microscopy in Geology. 2nd Edition. Cambridge; Cambridge University Press; 2010.
[14] Parkhurst DL, Appelo, CAJ. Description of Input and Examples for PHREEQC Version 3 – A Computer Program for Speciation, Batch-Reaction, One-Dimensional Transport, and Inverse Geochemical Calculations. Denver, Colorado; USGS Techniques and Methods: 2013.
[15] Wolery, TJ. EQ3/6, A Software Package for Geochemical Modeling of Aqueous Systems: Package Overview and Installation Guide (Version 7.0). Lawrence Livermore National Laboratory; 1992.
[16] Regenspurg S, Brand A, Peiffer S. Formation and stability of schwertmannite in acidic mining lakes. Geochim Cosmochim Acta 2004; 68(6): 1185-1197.
[17] Palandri JL, Kharaka YK. A Compilation of Rate Parameters of Water-Mineral Interaction Kinetics for Application to Geochemical Modeling. US Geological Survey Open File Report 2004-1068; 2004.
[18] Cantucci B, Montegrosso G, Vaselli O, Tassi F, Quatrocchi F, Perkins EH. Geochemical modeling of CO2 storage in deep reservoirs: The Weyburn Project (Canada) case study. Chem Geol 2009; 265: 181-197.
[19] Xu T, Apps JA, Pruess K. Mineral sequestration of carbon dioxide in a sandstone-shale system. Chem Geol 2005; 217: 295-318.
[20] Xu T, Apps JA, Pruess K, Yamamoto H. Numerical modeling of injection and mineral trapping of CO2 with H2S and SO2 in sandstone formations. Chem Geol 2007; 242: 319-346.
[21] Gautier JM, Oelkers EH, Schott J. Are quartz dissolution rates proportional to B.E.T. surface areas? Geochim Cosmochim Acta 2001; 65(7): 1059-1070.
[22] Steefel CI, Lichtner PC. Multicomponent reactive transport in discrete fractures II: Infiltration of hyperalkaline groundwater at Maqarin, Jordan, a natural analogue site. J Hydrol 1998; 209: 200-224.
[23] Cornell RM, Schwertmann U. The Iron Oxides. Weinheim; VCH Verlagsgesellschaft: 1996.
[24] Nordstrom DK, Alpers, CN. Negative pH, efflorescent mineralogy, and consequences for environmental restoration at the Iron Mountain Superfund site, California. Proc Natl Acad Sci USA 1999; 96: 3455-3462.